[32] W. Yin, S. Osher, D. Goldfarb, and J. Darbon. Bregman iterative algorithms for L1-minimization with applications to compressed sensing. *SIAM Journal on Imaging Sciences*, 1(1):143–168, 2008.

Mahdi Dodangeh
CMUC, Department of Mathematics, University of Coimbra
E-mail address: dodangeh@mat.uc.pt

Isabel Narra Figueiredo
CMUC, Department of Mathematics, University of Coimbra
E-mail address: isabelf@mat.uc.pt
URL: http://www.mat.uc.pt/∼isabelf/

Gil Gonçalves
INESCC and Department of Mathematics, University of Coimbra
E-mail address: gil@mat.uc.pt
URL: http://www.mat.uc.pt/∼gil/

Pré-Publicações do Departamento de Matemática
Universidade de Coimbra
Preprint Number 16–13

SPATIALLY ADAPTIVE TOTAL VARIATION DEBLURRING WITH SPLIT BREGMAN TECHNIQUE

MAHDI DODANGEH, ISABEL NARRA FIGUEIREDO AND GIL GONÇALVES

Abstract: In this paper we describe a modified non-blind and blind deconvolution model by introducing a regularization parameter that incorporates the spatial image information. Indeed, we have used a weighted total variation (TV) term, where the weight is a spatially adaptive parameter based on the image gradient. The proposed models are solved by the split Bregman method. To handle adequately the discrete convolution transform in a moderate time, fast Fourier transform is used. Tests are conducted on several images, and for assessing the results we define appropriate weighted versions of two standard image quality metrics. These new weighted metrics clearly highlight the advantage of the spatially adaptive approach.

Keywords: Deblurring, Convolution, Split Bregman method, Fast Fourier transform, Local quality measure.

1. Introduction

Deblurring is the process of reconstructing a sharp image from a given blurred image that is also possibly deteriorated with noise. Deblurring occurs frequently in a wide range of applications as remote sensing and medical imagery processing, astrophysics, signal processing, statistical inference, and optics. It is generally modeled as a convolution of the unknown true image (to be recovered) with a linear and shift invariant blur operator (also called the point spread function (PSF) or kernel), and therefore in this case the blurring process reduces to convolution and deblurring becomes also called deconvolution (see [8]).

There are three main types of deconvolution problems. (1) Blind deconvolution, which includes the cases when both kernel and true image are unknown. (2) Semi-blind deconvolution, in which the kernel belongs to a known class of parametric functions. (3) Non-blind deconvolution where only the

Received March 24, 2016.
This work was partially supported by the project PTDC/MATNAN/0593/2012, and also by CMUC (Center for Mathematics, University of Coimbra) and FCT (Portuguese national funding agency for science, research and technology), through European program COMPETE / FEDER and project PEst-C/MAT/UI0324/2013.

true image is unknown. The main challenge is that direct deconvolution is unstable and disturbed by noise present in the input blurred image.

An effective deconvolution method requires a balance between frequency recovery and noise suppression. A workaround to overcome this difficulty is the use of regularization methods to stabilize the solution. Tikhonov regularization [29] is one of the popular regularization techniques, in which a quadratic penalty is added to the objective function. Common choices for this quadratic penalty involve the identity or a matrix approximating the first or second order derivative operator [19, 20]. Total variation (TV) regularization is a successful technique for achieving the aforementioned balance in deblurring problems. In [27] TV is proposed for image denoising and then in [28] it is also applied to deconvolution. Blind deconvolution was first introduced by [10], and a lot of work has been carried out so far to improve the models introduced in [1, 9, 23]. An excellent tutorial has been provided by [21]. Despite a vast amount of research in the field (see [21] and references therein), the design of a principled, stable and robust algorithm that can handle real images remains a challenge.

We remark that by enforcing the TV regularization, one might lose some precious information at the edge pixels since the TV regularization makes the image smoother. In this paper to control this side effect, a spatially adaptive deconvolution model is proposed. Here, we constrain the TV regularization by the spatially adaptive information, by introducing a weighted TV term, whose weight depends on the gradient of the image. In edge pixels, a weak regularization strength is enforced to preserve detail, and in the homogeneous areas, an active regularization strength is enforced to recover a sharper image. Furthermore, we apply the split Bregman algorithm of Goldstein and Osher [16] to approximate the solution of the proposed spatially adaptive TV deconvolution problem.

We observe that the deconvolution problem belongs to a class of second order cone programming and thus could be solved via interior-point methods [3]. However, interior-point methods are not suitable for deconvolution since this latter involves non-sparse matrix data, which often prevents the use and latent benefits of modern interior-point methods. Another issue is that the minimization problem dimension can reach millions even for small images. These facts inspire the exploration of simpler and fast algorithms for deconvolution. In this paper, we use fast Fourier transform (FFT) to

[12] M.A.T. Figueiredo, R.D. Nowak, and S.J. Wright. Gradient projection for sparse reconstruction: Application to compressed sensing and other inverse problems. *Selected Topics in Signal Processing, IEEE Journal of*, 1(4):586–597, Dec 2007.

[13] P. Getreuer. Total Variation Deconvolution using Split Bregman. *Image Processing On Line*, 2:158–174, 2012.

[14] G. Gilboa and S. Osher. Nonlocal linear image regularization and supervised segmentation. *Multiscale Modeling & Simulation*, 6(2):595–630, 2007.

[15] G. Gilboa and S. Osher. Nonlocal operators with applications to image processing. *Multiscale Modeling & Simulation*, 7(3):1005–1028, 2009.

[16] T. Goldstein and S. Osher. The Split Bregman method for L1-regularized problems. *SIAM Journal on Imaging Sciences*, 2(2):323–343, 2009.

[17] R. C. Gonzalez and R. E. Woods. *Digital Image Processing (3rd Edition)*. Prentice-Hall, Inc., Upper Saddle River, NJ, USA, 2006.

[18] E. T. Hale, W. Yin, and Y. Zhang. Fixed-point continuation for ℓ_1-minimization: Methodology and convergence. *SIAM Journal on Optimization*, 19(3):1107–1130, 2008.

[19] P. Hansen. *Rank-Deficient and Discrete Ill-Posed Problems*. Society for Industrial and Applied Mathematics, 1998.

[20] P. C. Hansen and D. P. O'Leary. The use of the l-curve in the regularization of discrete ill-posed problems. *SIAM Journal on Scientific Computing*, 14(6):1487–1503, 1993.

[21] D. Kundur and D. Hatzinakos. Blind image deconvolution. *Signal Processing Magazine, IEEE*, 13(3):43–64, May 1996.

[22] S.A. Martucci. Symmetric convolution and the discrete sine and cosine transforms. *Signal Processing, IEEE Transactions on*, 42(5):1038–1051, May 1994.

[23] R. Molina, J. Mateos, and A.K. Katsaggelos. Blind deconvolution using a variational approach to parameter, image, and blur estimation. *Image Processing, IEEE Transactions on*, 15(12):3715–3727, Dec 2006.

[24] S. Osher, M. Burger, D. Goldfarb, J. Xu, and W. Yin. An iterative regularization method for total variation-based image restoration. *Multiscale Modeling & Simulation*, 4(2):460–489, 2005.

[25] S. Osher, Y. Mao, B. Dong, and W. Yin. Fast linearized Bregman iteration for compressive sensing and sparse denoising. *Commun. Math. Sci.*, 8(1):93–111, 03 2010.

[26] D. Perrone and P. Favaro. Total variation blind deconvolution: The devil is in the details. In *Proceedings of the 2014 IEEE Conference on Computer Vision and Pattern Recognition*, CVPR '14, pages 2909–2916, Washington, DC, USA, 2014. IEEE Computer Society.

[27] L. I. Rudin, S. Osher, and E. Fatemi. Nonlinear total variation based noise removal algorithms. *Phys. D*, 60(1-4):259–268, November 1992.

[28] L.I. Rudin and S. Osher. Total variation based image restoration with free local constraints. In *Image Processing, 1994. Proceedings. ICIP-94., IEEE International Conference*, volume 1, pages 31–35 vol.1, Nov 1994.

[29] A. N. Tikhonov and V. Y. Arsenin. *Solutions of ill-posed problems*. V. H. Winston, Washington, DC, 1977.

[30] Z. Wen, W. Yin, D. Goldfarb, and Y. Zhang. A fast algorithm for sparse reconstruction based on shrinkage, subspace optimization, and continuation. *SIAM Journal on Scientific Computing*, 32(4):1832–1857, 2010.

[31] J. Yang and Y. Zhang. Alternating direction algorithms for ℓ_1-problems in compressive sensing. *SIAM Journal on Scientific Computing*, 33(1):250–278, 2011.

up the discrete deconvolution process fast Fourier transform is used. The numerical experiments demonstrate the good performance of the proposed models, that is evaluated in terms of standard and appropriate weighted quality metrics. In particular the appropriate weighted metrics, proposed in this paper, clearly demonstrate the superiority of the spatially adaptive deblurring models. However, the proposed models depend on several parameters, that are fixed manually. In the future, we intend to address these parameter related issues and in particular to perform a deep study to find the optimal parameters, in an automatic way.

Acknowledgment

This work was supported in part by the Portuguese National Funding Agency for Science, Research and Technology (FCT) under Project PTDC/MATNAN/0593/2012, and PEst-OE/EEI/UI308/2014, and in part by CMUC – UID/MAT/00324/2013, funded by FCT/MCTES (Portugal) and co-funded by the European Regional Development Fund through the Partnership Agreement PT2020.

References

[1] M.S.C. Almeida and L.B. Almeida. Blind and semi-blind deblurring of natural images. *Image Processing, IEEE Transactions on*, 19(1):36–52, Jan 2010.

[2] A. Beck and M. Teboulle. A fast iterative shrinkage-thresholding algorithm for linear inverse problems. *SIAM Journal on Imaging Sciences*, 2(1):183–202, 2009.

[3] A. Ben-Tal and A. Nemirovski. *Lectures on Modern Convex Optimization*. Society for Industrial and Applied Mathematics, 2001.

[4] E. Berg and M.P. Friedlander. Probing the Pareto frontier for basis pursuit solutions. *SIAM Journal on Scientific Computing*, 31(2):890–912, 2009.

[5] L. M. Bregman. The relaxation method of finding the common point of convex sets and its application to the solution of problems in convex programming. *USSR Computational Mathematics and Mathematical Physics*, 7(3):200–217, 1967.

[6] J.-F. Cai, S. Osher, and Z. Shen. Convergence of the linearized Bregman iteration for ℓ_1-norm minimization. *Mathematics of Computation*, 78(268):2127–2136, 2009.

[7] J.-F. Cai, S. Osher, and Z. Shen. Linearized Bregman iterations for compressed sensing. *Mathematics of Computation*, 78(267):1515–1536, 2009.

[8] T. F. Chan and J. J. Shen. *Image processing and analysis: variational, PDE, wavelet, and stochastic methods*. SIAM, 2005.

[9] T. F. Chan and C.K. Wong. Convergence of the alternating minimization algorithm for blind deconvolution. *Linear Algebra and its Applications*, 316(13):259 – 285, 2000. Special Issue: Conference celebrating the 60th birthday of Robert J. Plemmons.

[10] T.F. Chan and C.K. Wong. Total variation blind deconvolution. *Image Processing, IEEE Transactions on*, 7(3):370–375, Mar 1998.

[11] P. L. Combettes and J.-C. Pesquet. Proximal thresholding algorithm for minimization over orthonormal bases. *SIAM Journal on Optimization*, 18(4):1351–1376, 2008.

solve the corresponding different minimization problems that arise in the split Bregman technique.

In order to evaluate the performance of the proposed methods we define weighted versions of two standard quality metrics (the average gradient and entropy) to act locally at the edge pixels. In addition we also compare the results of the proposed spatially adaptive blind deblurring method with the state-of-the-art method [26]. All the obtained results, evaluated with the aforementioned weighted and standard quality metrics, indicate the advantage of the spatially adaptive proposed methods.

After this introduction, the rest of the paper is organized as follows: Sections 2 and 3 describe the usual and the proposed (spatially adaptive) deblurring models (non-blind and blind cases). The solution of the spatially adaptive models, using the split Bregman method, is reported in Section 4. The obtained results of the experimental tests are described in Section 5 and finally in the last section we draw some conclusions and future research directions.

2. Non-Blind and Blind Deblurring Models

A blurred image f (herein identified with a function $f : \Omega \to \mathbb{R}$, where $\Omega \subset \mathbb{R}^2$ is the pixel domain) corrupted with additive Gaussian noise z can be defined as

$$f \;=\; \varphi * u + z.$$

Here $\varphi : \Omega \to \mathbb{R}$ represents the blur operator (a linear shift invariant function, known as the point spread function (PSF) or kernel), which is known in the non-blind model and unknown in the blind model. The unknown sharp image, to be recovered, is represented by $u : \Omega \to \mathbb{R}$ and finally $*$ stands for the convolution operator.

As stated in [10] a variational formulation for the corresponding non-blind deblurring problem is

$$\min_u \left(\frac{\alpha_u}{2} \|\varphi * u - f\|^2_{L^2(\Omega)} + TV(u) \right), \tag{1}$$

and for the blind deblurring problem is

$$\min_{u,\varphi} \left(\frac{\alpha_u}{2} \|\varphi * u - f\|^2_{L^2(\Omega)} + TV(u) + \alpha_\varphi TV(\varphi) \right). \tag{2}$$

Here $L^2(\Omega)$ is the space of square integrable functions in Ω, with norm denoted by $\|.\|_{L^2(\Omega)}$. The constants α_u and α_φ are two positive parameters

which balance the influence of the matching and regularizing terms in the cost functions. The total variation of u, $TV(u)$ (respectively $TV(\varphi)$), is a semi-norm, that when u (respectively φ) is smooth is equivalent to the integral of the gradient magnitude of u (respectively φ)

$$TV(u) = \int_{\Omega} |\nabla u| dx = \|\nabla u\|_{L^1(\Omega)}$$

where $L^1(\Omega)$ is the space of absolutely integrable functions in Ω, with norm denoted by $\|.\|_{L^1(\Omega)}$, and ∇ represents the gradient operator.

The TV regularization is an effective regularization approach for recovering edges of an image and this is the main motivation, as explained in [10] for using TV regularization in model (1), and also in model (2), since some PSF can have edges (as for instance motion blur or out-of-focus blur that are piecewise constant functions with discontinuities).

The blind deconvolution model (2) is not convex. However, with φ or u fixed it becomes convex and consequently the non-blind model (1) is convex. So a solution to problem (2) can be readily found by an iterative algorithm that alternates between the estimation of the image u, given the kernel φ, and the estimation of the kernel, given the image. This approach is called alternating minimization (AM) [10]. In [10] it is suggested a variant of the AM algorithm that employs a gradient descent scheme for each step. Then, several well-known approaches in this area are applied to the model, as for example the gradient projection method [12], the fixed-point continuation method [18], the spectral projected gradient method [4], and the Bregman iterative method [6, 7, 24, 25, 32]. The most recent schemes can be found in [2, 11, 30, 31].

3. Modified Deblurring Models

Here we present a modification of the models (1) and (2) by introducing a weighted TV, for the regularizing term in u, with a weight function $w_u(x)$ (where x represents an arbitrary point in the pixel domain Ω), depending on u, more precisely on the gradient of u. The modified deblurring models, respectively non-blind and blind, are defined by (supposing hereafter that u and φ are smooth)

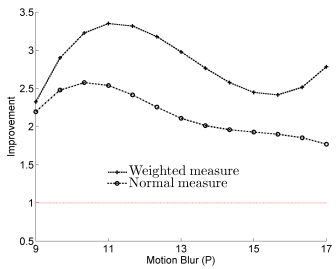

FIGURE 7. Evaluation of the modified blind deblurring model for the EO image: comparison of the improvement with respect to the Perrone *et al.* method [26], based on the outputs of Table 4 and using the quantities defined in (12).

proposed method recovers a better image compared to the image obtained with Perrone *et al.* method [26] and with a significant improvement.

We remark that we have also done the assessment, of the performance of all the results reported in this section, with other evaluation metrics different from SNR and GNR. Namely, we have used PSNR (peak signal to noise ratio) and PSNRG (peak signal to noise ratio of the gradient) and defined the corresponding weighted measures, applying the same weight introduced before for the weighted measures WSNR and WSNRG. However, the results were more or less the same as the reported results. Finally, we also point out that the numerical tests also show that the quality of the results depend on the parameters involved in the definition of the model. For instance, α_φ and λ_φ should be relatively small compared to λ_u, and λ_φ should be bigger than α_φ. On the other hand the size of α_u should be relatively big compared to λ_u. Thus the choice of these parameter requires a careful decision. This is an issue that we did not analyse in the present paper but we intend to address as future work.

6. Conclusion

We have presented a modified version for non-blind and blind deblurring models based on the local information. More precisely, in these new models, there is a weighted Total Variation (TV) regularization term, that is constrained by the spatially adaptive information. The split Bregman optimization algorithm is employed to solve the proposed models. To speed

		SNR	SNRG	WSNR	WSNRG
	Input	19.14	0.53	14.25	0.63
P=17	Proposed	26.63	8.85	24.00	14.32
	Perrone *et al.*	23.37	3.22	17.75	5.01
	Input	19.59	0.63	14.55	0.74
P=15	Proposed	28.90	10.35	26.08	15.81
	Perrone *et al.*	24.42	4.08	19.26	6.28
	Input	20.13	0.77	14.93	0.90
P=13	Proposed	30.15	11.15	27.50	17.26
	Perrone *et al.*	24.89	4.41	19.15	6.84
	Input	20.77	0.97	15.40	1.12
P=11	Proposed	33.26	13.28	30.76	19.49
	Perrone *et al.*	25.69	5.05	19.99	7.78
	Input	21.60	1.25	16.04	1.47
P=9	Proposed	33.47	13.59	30.68	19.10
	Perrone *et al.*	27.01	6.31	22.34	9.83
	Input	22.69	1.75	16.97	2.14
P=7	Proposed	37.49	16.49	35.96	24.03
	Perrone *et al.*	24.59	3.96	16.35	7.38

TABLE 4. Evaluation measures for the EO image.

involving the weighted and normal measures, and based on the outputs shown in Table 4. In Figure 7 these outputs are analysed by computing the quantity

$$\frac{\mathrm{M}_{sa}-\mathrm{M}_{in}}{\mathrm{M}_{tv}-\mathrm{M}_{in}}, \tag{11}$$

where the quality measure M is SNR or WSNR, and the lower subscripts indicate that the measure is taken from the output (of the proposed method (sa) or Perrone *et al.* method (tv)) or from the input blurred image (in). More exactly, in Figure 7 we use

$$\frac{\mathrm{WSNR}_{sa}-\mathrm{WSNR}_{in}}{\mathrm{WSNR}_{tv}-\mathrm{WSNR}_{in}} \quad \text{and} \quad \frac{\mathrm{SNR}_{sa}-\mathrm{SNR}_{in}}{\mathrm{SNR}_{tv}-\mathrm{SNR}_{in}}. \tag{12}$$

The quantities (12) (weighted and normal) evaluate the relative improvement of the proposed blind deblurring (spatially adaptive) method with respect to the Perrone *et al.* method [26]. From Figure 7, we conclude that the

$$\min_{u}\left(\frac{\alpha_u}{2}\|\varphi*u-f\|^2_{L^2(\Omega)}+\underbrace{\|w_u\nabla u\|_{L^1(\Omega)}}_{TV_{w_u}(u)}\right),$$

$$\min_{u,\varphi}\left(\frac{\alpha_u}{2}\|\varphi*u-f\|^2_{L^2(\Omega)}+\underbrace{\|w_u\nabla u\|_{L^1(\Omega)}}_{TV_{w_u}(u)}+\alpha_\varphi\underbrace{\|\nabla\varphi\|_{L^1(\Omega)}}_{TV(\varphi)}\right).$$

The main idea is that in edges pixels, a weak regularization is enforced to better preserve edges and in homogeneous regions a strong regularization is enforced to recover a sharp image. The definition of this spatially adaptive parameter $w_u(x)$, which controls the amount of regularization in u, is

$$w_u(x)=\frac{1}{1+\|\nabla u(x)\|^2/\eta}, \quad \text{with} \quad \eta=\gamma std(\|\nabla u\|^2) \tag{3}$$

where $\|.\|$ is the Euclidean norm and η is a non-negative parameter, which is set to a constant (γ) times the standard deviation std, of the gradient of the exact image. Therefore the larger the gradient $\|\nabla u(x)\|$ is, at pixel x, the smaller the corresponding parameter $w_u(x)$, and consequently little regularization is applied to preserve detail.

4. Split Bregman Method for the Modified Deblurring Models

Regularizaton of the deblurring model is an important procedure for the obtention of a stable solution. The advantage of the L^1-regularization over the L^2-regularization is that as opposed to the latter, the L^1-regularization is less sensitive to outliers. However, the L^1-regularization makes the model non-smooth. To benefit the advantage of the L^1-regularization and for reducing its inherent difficulties we have used the split Bregman scheme [16]. In this scheme, the goal is to separate entirely the L^1-regularizing term and the L^2-matching term in each subproblem. Then we enforce these constraints with the Bergman iteration process [5]. By doing so, we will have minimization subproblems to solve at each alternating step.

4.1. Modified Non-Blind Model. First an extra variable d_u is introduced through the constraint

$$d_u = \nabla u$$

with the goal of completely separating the L^1 and L^2 terms. This constraint is enforced by the Bregman iteration process [5]. Therefore the following sequence of minimization problems are considered: For $k = 1, 2, \ldots$ find (u^{k+1}, d_u^{k+1}) solution of

$$\begin{cases} \min\limits_{(u,d_u)} \Big(\dfrac{\alpha_u}{2}\|\varphi * u - f\|^2_{L^2(\Omega)} + \|w_u d_u\|_{L^1(\Omega)} \\ \qquad\qquad + \frac{\lambda_u}{2}\|d_u - \nabla u - b_u^k\|\Big) \\ b_u^{k+1} = b_u^k - d_u^{k+1} + \nabla u^{k+1}, \end{cases} \tag{4}$$

where λ_u is the fixed penalty parameter resulting from the Bregman approach.

The minimization problem in (4) can be solved by an alternating minimization algorithm, by minimizing with respect to u and d separately. Briefly, the overall Split Bregman procedure can be summarized as follows:

Non-Blind Deblurring Algorithm (NBDA):

Input:

f and φ.

while $\max\{|u^k - u^{k-1}|\} > tol$ (with tol a pre-fixed tolerance) **do**

$$u^{k+1} = \mathcal{F}^{-1}\left(\frac{\alpha_u \overline{\mathcal{F}(\varphi)} \cdot \mathcal{F}(f) - \lambda_u \mathcal{F}\big(div(d^k - b^k)\big)}{\alpha_u |\mathcal{F}(\varphi)|^2 - \lambda_u\, \mathcal{F}(\Delta)}\right)$$

$$w_{u^{k+1}}(x) = \frac{1}{1 + \|\nabla u^{k+1}(x)\|^2/\eta},$$

$$\eta = \gamma\, std(\|\nabla u^{k+1}\|^2),$$

$$d_u^{k+1} = \text{shrink}(\nabla u^{k+1} + b^k, \frac{w_{u^{k+1}}}{\lambda_u})$$

$$b_u^{k+1} = b_u^k - d_u^{k+1} + \nabla u^{k+1}.$$

end while

Output:

Recovered image u^{k+1}.

		SNR	SNRG	WSNR	WSNRG
MI	Input	29.01	1.71	11.36	1.74
	Proposed	37.68	8.70	26.54	19.50
	Perrone *et al.*	33.60	4.44	15.28	8.70
EO	Input	22.11	1.32	16.53	1.66
	Proposed	35.47	14.50	33.65	22.03
	Perrone *et al.*	24.75	3.44	19.77	5.98

TABLE 3. Quality measures for MI and EO images

display the values of the quality (standard/global and weighted/local) measures: SNR, SNRG, WSNR and WSNRG.

UAV imagery is at an increasing use in remote sensing community due to its high ground resolution and good spectral resolution. To achieve this UAVs flew at low flight altitudes and are equipped with small height and high-resolution cameras. However due to the camera movement during image acquisition UAV imagery is often contaminated with motion blur. So in the next experiments, we have considered the EO image, blurred it with several motion blur kernels, such that P= 17, 15, 13, 11, 9 and 7 pixels. Then we have applied the deblurring algorithm described at the end of Section 4.2. We set the parameters to be

in the BDA Algorithm (first iterate)
$\alpha_u = 100 \quad \lambda_u = 4 \quad \alpha_\varphi = 10^{-5} \quad \lambda_\varphi = 4 \times 10^{-1}$,

in the NBDA Algorithm (first iterate)
$\alpha_u = 2 \times 10^3 \quad \lambda_u = 7$,

in the BDA Algorithm (second iterate)
$\alpha_u = 10^5 \quad \lambda_u = 1 \quad \alpha_\varphi = 10^{-4} \quad \lambda_\varphi = 4 \times 10^{-1}$,

in the NBDA Algorithm (second iterate)
$\alpha_u = 7 \times 10^4 \quad \lambda_u = 6$.

The corresponding results are displayed in Table 4 and show that the proposed method performs better than the Perrone *et al.* method [26]. The organization of Table 4 is the same that was explained for Table 3, except that now the first column refers to the value of the motion blur pixel P.

Finally, Figure 7 shows the improvement obtained with our blind deblurring (spatially adaptive) model, for the EO image, by using appropriate quantities

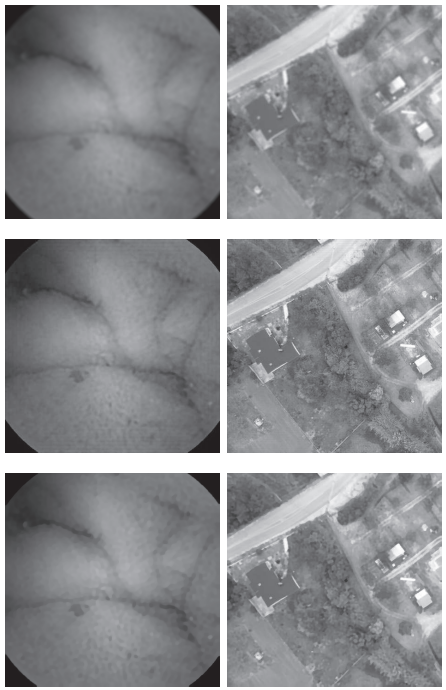

FIGURE 6. First column (form top to bottom): MI image corrupted by an out-of-focus blur with radius R=5 (right), the recovered image with the proposed BDA method (using $\alpha_\varphi = 10^{-5}$, $\lambda_\varphi = 4 \times 10^{-3}$, $\alpha_u = 5 \times 10^6$, $\lambda_u = 0.6$) and with the method by Perrone *et al.* [26]. Second column (form top to bottom): EO image blurred by an out-of-focus blur with radius R=3, the recovered image by the proposed BDA method (using $\alpha_\varphi = 10^{-5}$, $\lambda_\varphi = 4 \times 10^{-3}$, $\alpha_u = 1.7 \times 10^6$, $\lambda_u = 1$) and with the method by Perrone *et al.* [26].

The results, corresponding to Figure 6, in terms of the previously defined standard measures and modified weighted versions, are reported in Table 3, where the columns are organized as follows: the first column exhibits the figure names, the second column the image names and the third to sixth columns

Here $\mathcal{F}$ denotes the fast Fourier transform, "." the pointwise multiplication, $\overline{\mathcal{F}(.)}$ the complex conjugate of $\mathcal{F}(.)$, *div* the divergence operator and $\mathcal{F}(\Delta)$ is the discrete Fourier transform (DFT) of the 5-point Laplacian (Δ) filter. The operator shrink is defined by $\text{shrink}(z, v) = \frac{z}{|z|} \cdot \max(|z| - v, 0)$, for any z, v in $\mathbb{R}$.

4.2. Modified Blind Model. The Split Bregman technique for the modified blind model follows the same pattern as in the case of the modified non-blind model. We first introduce two extra variables to separate the L^1 and L^2 terms, that is

$$d_u = \nabla u, \qquad d_\varphi = \nabla \varphi$$

and enforce these constraints by the Bregman iteration procedure, such that the following sequence of minimization problems are obtained: for $k = 1, 2, \ldots$ find $(u^{k+1}, d_u^{k+1}, \varphi^{k+1}, d_\varphi^{k+1})$ solution of

$$\begin{cases} \min\limits_{(u,d_u,\varphi,d_\varphi)} \Big(\dfrac{\alpha_u}{2} \|\varphi * u - f\|^2_{L^2(\Omega)} + \|w_u d_u\|_{L^1(\Omega)} \\ \qquad\qquad + \alpha_\varphi \|d_\varphi\|_{L^1(\Omega)} + \frac{\lambda_u}{2} \|d_u - \nabla u - b_u^k\| \\ \qquad\qquad\qquad + \frac{\lambda_\varphi}{2} \|d_\varphi - \nabla\varphi - b_\varphi^k\| \Big), \\ b_u^{k+1} = b_u^k - d_u^{k+1} + \nabla u^{k+1}, \\ b_\varphi^{k+1} = b_\varphi^k - d_\varphi^{k+1} + \nabla \varphi^{k+1}. \end{cases} \tag{5}$$

The solution of the minimization problem in (5) can be solved by minimizing iteratively and separately with respect to u^{k+1}, d_u^{k+1}, φ^{k+1}, d_φ^{k+1}.

Similarly to [10], in order to obtain a physical solution we impose, during the algorithmic procedure the following conditions on u and φ

$$\begin{aligned} &\|\varphi\|_{L^1(\Omega)} = 1, \quad u(x), \quad \varphi(x) \geq 0 \\ &\varphi^-(x) = \varphi(x) \quad (\varphi \text{ is centre-symmetric}), \end{aligned} \tag{6}$$

where $\varphi^-(x) = \varphi(-x)$.

Summarizing, given the blurred image f, the size of the kernel $[m, n]$, and an initial guess u^0 of the sharp image, the proposed spatially adaptive blind deconvolution Split Bregman procedure is the following :

Blind Deblurring Algorithm (BDA):

Input:

f, $[m, n]$=size of the kernel φ and u^0.

Initialize:

$\varphi^0 = \dfrac{1}{m \times n}$.

while $\max\{|u^k - u^{k-1}|, |\varphi^k - \varphi^{k-1}|\} > tol$ (with tol a pre-fixed tolerance) **do**

Kernel part:

$$\varphi^{k+1} = \mathcal{F}^{-1}\left(\frac{\alpha_u \overline{\mathcal{F}(u^k)} \cdot \mathcal{F}(f) - \lambda_\varphi \mathcal{F}(div(d_u^k - b_u^k))}{\alpha_u |\mathcal{F}(u^k)|^2 - \lambda_\varphi \mathcal{F}(\Delta)}\right)$$

$$\varphi^{k+1} = \frac{\varphi^{k+1} + \varphi^{k+1^-}}{2}$$

$$\varphi^{k+1} = \max\{\varphi^{k+1}, 0\}$$

$$\varphi^{k+1} = \frac{\varphi^{k+1}}{\|\varphi^{k+1}\|_{L^1(\Omega)}}$$

$$d_\varphi^{k+1} = \text{shrink}(\nabla\varphi^{k+1} + b_\varphi^k, \alpha_\varphi/\lambda_\varphi)$$

$$b_\varphi^{k+1} = b_\varphi^k - d_\varphi^{k+1} + \nabla\varphi^{k+1}$$

Image part:

$$u^{k+1} = \mathcal{F}^{-1}\left(\frac{\alpha_u \overline{\mathcal{F}(\varphi^{k+1})} \cdot \mathcal{F}(f) - \lambda_u\, \mathcal{F}(div(d_u^k - b_u^k))}{\alpha_u |\mathcal{F}(\varphi^{k+1})|^2 - \lambda_u \mathcal{F}(\Delta)}\right)$$

$$u^{k+1} = \max\{u^{k+1}, 0\}$$

$$w_{u^{k+1}}(x) = \frac{1}{1 + \|\nabla u^{k+1}(x)\|^2/\eta},$$

$$\eta = \gamma std(\|\nabla u^{k+1}\|^2)$$

$$d_u^{k+1} = \text{shrink}(\nabla u^{k+1} + b_u^k, w_{u^{k+1}}/\lambda_u)$$

$$b_u^{k+1} = b_u^k - d_u^{k+1} + \nabla u^{k+1}$$

end while

Output:

Recovered image u^{k+1} and kernel φ^{k+1}.

Similarly to (8) and (9), the quantities (10) evaluate the relative improvement of the difference of the weighted measures, for the spatially adaptive and non-adaptive methods, with respect to the difference of the global measures for the spatially adaptive and non-adaptive methods.

The Figure 5 exhibits the results obtained with (10), and using the outputs displayed in Tables 1 - 2. It demonstrates the advantage of the spatial approach (in fact in all the cases the curves are above the horizontal line which means no improvement) and the suitability of the weighted measures. The first and second rows in Figure 5 correspond to the results of Table 1 and the third and fourth rows to those of Table 2. The first column in Figure 5 shows the curves for the left quantity in (10), the second column displays the curves for the right quantity represented in (10).

5.3. Evaluation of the Modified Blind Model. In these second tests we evaluate the blind deconvolution deblurring algorithm (BDA) by comparing its performance with the method proposed by Perrone *et al.* [26]. We have selected this state-of-the-art method because its affinities with our blind deblurring method, the differences with respect to the solving technique, and because of the crucial difference (it is not spatially adaptive like the method we are proposing in this paper), that is :

- It is also a blind deconvolution model regularized by total variation (TV).
- Like our method, it exploits the benefit of alternating between non-blind and blind procedures.
- It uses a steepest decent procedure, while our proposed model is based on FFT (fast Fourier Transform).
- Unlike our method, it does not include any spatially adaptive parameter while our approach is spatially adaptive.

Figure 6 shows the results of our modified blind deblurring method (spatial adaptive) applied to the medical image MI and the EO image, as well as the results obtained with the method proposed by Perrone *et al.* [26], for comparison. We have used the suggested parameters indicated in Perrone *et al.* [26] as well as the implementation of a pyramid scheme (the image u and the blur φ are down-sampled until the latter has the size 3×3 pixels; then, for the lowest scale, the algorithm is executed, and the up-sampled (or down-sampled) results are used as initializations for the following scale).

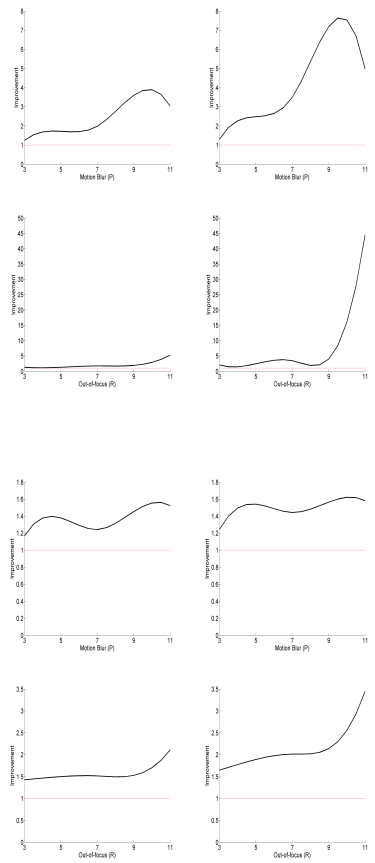

FIGURE 5. Evaluation of the modified non-blind deblurring method: comparison of the relative improvement of the spatially adaptive approach on the non-adaptive one. First and second rows correspond to the synthetic image and the third and fourth rows to the standard test image. Curves for the left quantity in (10) are displayed in the first column, and the curves for the right quantity displayed in (10) are shown in the second column.

We remark that in all the experiments, either for the modified non-blind or blind deblurring algorithms, in order to reduce artifacts at the boundary, we extend the image to be zero at the boundary. More precisely, we introduce four narrow strips around the boundary of the pixel domain with pixel values equal to zero. We denote that extension by Eu. Then the discrete convolution is implemented through the discrete Fourier transform (DFT) as

$$\varphi * u \;=\; \mathcal{F}^{-1}\left(\mathcal{F}(\varphi)\cdot\mathcal{F}(Eu)\right).$$

When the image u and the blur operator φ are even (an even function g verifies $g(x) = g(-x)$), using cosine discrete transform (CDT) instead of FFT will reduce the expense of each iteration (see [13, 22]).

Furthermore, for the modified blind deblurring algorithm, we realized experimentally that to recover a sharp image, α_u should be relatively big, compared to other parameters. But, a big α_u usually destroys the quality of the recovered kernel. To overcome this difficulty, we alternate between the blind and non-blind procedures. After recovering a kernel in the BDA method, we executed the NBDA using the previous recovered kernel to restore a sharp image. Then, we passed the recovered image to the BDA procedure to obtain a better kernel. Usually, we have observed that two or three times alternating is enough to recover both a sharp image and kernel. This alternating process also prevents to stick around a local minimizer. Summarizing, in the experiments reported in Section 5, we have implemented the following blind deblurring algorithm.

Deblurring Algorithm (reformulation)

Input:
f and $[m, n]$=size of the kernel φ.

Initialize:
$u^0 = Ef$.

for $i = 0, 1, 2, \ldots$ **do**
φ^{i+1} is obtained with BDA (inputs - f, [m,n], u^i)
u^{i+1} is obtained with NBDA (inputs - f, φ^{i+1})
end for

Output:
Recovered image u^{i+1} and kernel φ^{i+1}.

5. Experimental Tests

For the tests we have used four different images that are displayed in Figure 1. The two images in the first row represent a synthetic and a standard test image. The second row shows, on the left, the grayscale version of a medical image (MI) of the small bowel, acquired with the wireless capsule Pillcam SB of the company *Given Imaging*. On the right it exhibits the grayscale version of an EO (earth observation) image, obtained with an Unmanned Aerial Vehicle (UAV) equipped with a consumer grade digital camera (Canon IXUS 127 HS) and flying at an altitude of $143\,m$ above ground level.

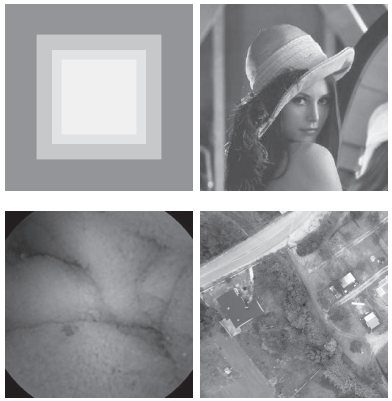

FIGURE 1. Images used in the tests. First row: left - synthetic image (256×256 pixels); right - standard test image (256×256 pixels). Second row: left - MI image (466×466 pixels); right - EO image (466×466 pixels).

We have done two types of tests. In the first type the goal is the evaluation and comparison of the performance of the spatially adaptive and non-adaptive approaches, for the non-blind deblurring algorithm. Here we only report the results for the synthetic and standard test images exhibited in the first row of Figure 1. The second tests consist in the evaluation and comparison of the performance of the modified blind deblurring algorithm (spatially adaptive) with a state-of-the-art method [26] (that is not spatially adaptive). In these second tests we report the results with the two genuine and real-life images, MI and EO, displayed in the second row of Figure 1.

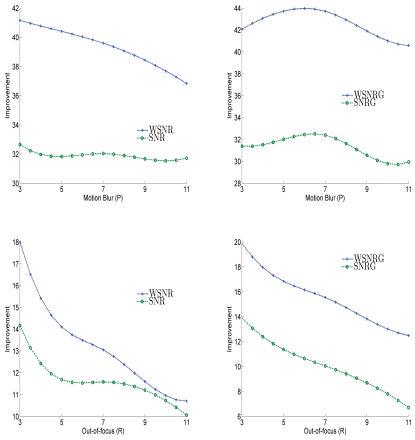

FIGURE 4. Comparison of the improvement of the reconstructed standard test image, in the edge pixels relatively to the reconstruction in the whole domain, for the spatially adaptive method. The curves represent the quantities defined by (8) on the left column and by (9) on the right column (the green color corresponds to the quantities involving the weighted measures whereas the blue one to the normal measures)

(global) SNR and SNRG measures. The Figures 3 and 4 clearly show that the weighted measure values are higher than the values of the normal measures. So the weighted metrics are appropriate to quantify the improvement obtained with the spatially adaptive approach. Consequently this means that at the edge pixels the image reconstruction is better with the spatially adaptive approach.

Likewise, to analyze the outputs, and compare the improvement of the spatially adaptive approach versus the non-adaptive one, we can also compute the following quantity

$$\frac{(\mathrm{WM}_{sa} - \mathrm{WM}_{in}) - (\mathrm{WM}_{na} - \mathrm{WM}_{in})}{(\mathrm{M}_{sa} - \mathrm{M}_{in}) - (\mathrm{M}_{na} - \mathrm{M}_{in})} = \frac{\mathrm{WM}_{sa} - \mathrm{WM}_{na}}{\mathrm{M}_{sa} - \mathrm{M}_{na}},$$

where M is SNR or SNRG. More precisely

$$\frac{\mathrm{WSNR}_{sa} - \mathrm{WSNR}_{na}}{\mathrm{SNR}_{sa} - \mathrm{SNR}_{na}} \text{ and } \frac{\mathrm{WSNRG}_{sa} - \mathrm{WSNRG}_{na}}{\mathrm{SNRG}_{sa} - \mathrm{SNRG}_{na}}. \tag{10}$$

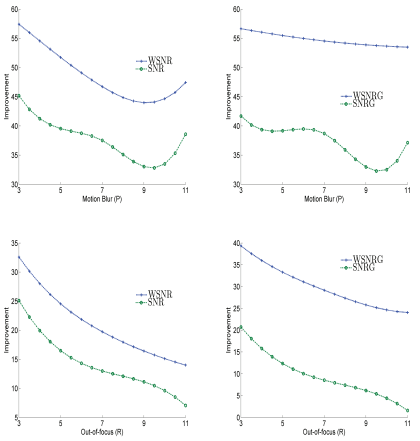

FIGURE 3. Comparison of the improvement of the reconstructed synthetic image, in the edge pixels relatively to the reconstruction in the whole domain, for the spatially adaptive method. The curves represent the quantities defined by (8) on the left column and by (9) on the right column (the blue color corresponds to the quantities involving the weighted measures whereas the green one to the normal measures).

where M is one of the quality measures SNR, SNRG, WSNR, or WSNRG of Section 5.1. The lower subscripts indicate that the measure is taken from the $out \in \{sa, na\}$ (the non-blind spatially adaptive model (sa) and non-adaptive one (na)) and the input blurred image (in). The bigger (7) is, the better is the reconstructed image.

Figures 3 and 4 exhibit the curves obtained with the quantities (weighted, denoted by W, and normal)

$$\mathrm{WSNR}_{sa} - \mathrm{WSNR}_{in} \quad \text{and} \quad \mathrm{SNR}_{sa} - \mathrm{SNR}_{in} \tag{8}$$

and

$$\mathrm{WSNRG}_{sa} - \mathrm{WSNRG}_{in} \quad \text{and} \quad \mathrm{SNRG}_{sa} - \mathrm{SNRG}_{in} \tag{9}$$

based on the results of Tables 1 and 2, respectively. The quantities (8) and (9) compute the improvement of the spatially adaptive method in terms of the weighted WSNR and WSNRG measures and those of the normal

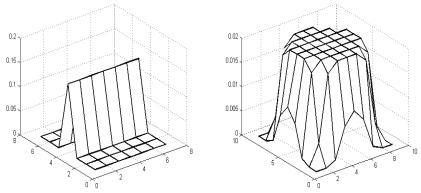

FIGURE 2. Left : Motion blur kernel with $P = 7$. Right : Out-of-focus blur kernel with $R = 4$.

For assessing the results we have used two standard quality measures as well as appropriate weighted modified versions of these measures, to highlight the advantage of the spatially adaptive model.

In all the tests the blurred images are distortions of the aforementioned four images, shown in Figure 1. These distorted images are obtained by using known blur operators. We have chosen two different types of blur kernels (see Figure 2). One simulates motion blur, of length P pixels at an angle ρ (in the experiments $\rho = 0$). The other simulates out-of-focus blur and is characterized by a disk-shaped kernel, denoted by φ, of radius R pixels, such that $\varphi(x) = 1/\pi R^2$, if $\|x\| < R$ and $\varphi(x) = 0$ otherwise.
Hereafter we always denote by P the number of pixels of a motion kernel and by R the radius in pixels of an out-of-focus kernel. Large P or R will lead to more blurred images.

5.1. Quality measures. For evaluating the quality of the results we have used the following two measures: Signal-to-noise ratio (SNR) and Signal-to-noise ratio of the Gradient (SNRG). SNR is defined in decibels as the ratio of the average power of a signal P_{signal} (meaningful information) to the average power of background noise P_{noise} (unwanted signal) (see [17]):

$$\mathrm{SNR} = 10 \log_{10} \left(\frac{P_{\text{signal}}}{P_{\text{noise}}} \right).$$

Generally, a large SNR indicates that the image reconstruction is of high quality. Likewise we define now SNRG (in decibels) as the ratio of the average power of gradient signal PG_{signal} (meaningful gradient) to the average power

of background noise in gradient PG_{noise} (unwanted gradient):

$$\text{SNRG} = 10\log_{10}\left(\frac{PG_{\text{signal}}}{PG_{\text{noise}}}\right).$$

Generally, a large SNRG indicates that the image reconstruction is of high quality.

To evaluate the quality of the reconstruction in the edges, we have modified the aforementioned measures by giving more weight to the edge pixels. The logic that we use here is similar to the one employed, for different purposes and meaning, in image processing areas (see *e.g.* [14, 15]). To be more precise, let β be a non-negative function such that $\|\beta\|_{L^1(\Omega)} = 1$, hereafter referred as the weight. For a grayscale image u, we set the weight β to be equal to β_u where

$$\beta_u(x) \;=\; \frac{1}{\|\nabla u\|^2}\nabla u(x)^\top \cdot \nabla u(x), \quad x \in \Omega.$$

Clearly this weight privileges edge pixels and is almost zero in flat or homogeneous regions of the image. Then, the weighted SNR (WSNR) and weighted SNRG (WSNRG), are defined by, respectively

$$\text{WSNR} \;=\; 10\log_{10}\left(\frac{WP_{\text{signal}}}{WP_{\text{noise}}}\right)$$

and

$$\text{WSNRG} = 10\log_{10}\left(\frac{WPG_{\text{signal}}}{WPG_{\text{noise}}}\right),$$

where in these fractions the weight β is involved.

5.2. Evaluation of the Modified Non-Blind Model. For these first tests, we consider the two scalar images displayed in the first row of Figure 1. The goal is to compare the results obtained with the non-blind deblurring algorithm NBDA, for the spatially adaptive case (when the parameter w_u is active and defined by (3)), and for the non-adaptive case (when $w_u = 1$). The results obtained for the top left and right images in Figure 1 are displayed in Tables 1 and 2, respectively. The rows (in), (sa), and (na) correspond, respectively, to the values of the measures for the input blurred image (in), the recovered images obtained with the spatially adaptive (sa) non-blind algorithm, and the non-adaptive (na) non-blind algorithm, respectively. These

		Motion Blur					Out-of-Focus Blur				
		R=2	R=3	R=4	R=5	R=6	P=3	P=5	P=7	P=9	P=11
SNR	(in)	37.13	34.58	33.03	31.91	31.02	33.70	31.67	30.34	29.33	28.51
	(sa)	82.30	74.12	70.56	64.94	69.60	58.79	48.16	43.32	40.45	35.58
	(na)	81.25	73.44	70.05	64.72	69.12	58.09	47.63	42.87	40.00	35.40
SNRG	(in)	9.49	5.49	4.55	4.12	3.86	5.26	2.86	1.96	1.49	1.20
	(sa)	52.25	45.32	43.82	37.34	41.55	26.01	15.22	10.50	7.68	2.80
	(na)	51.18	44.65	43.26	37.09	41.00	25.35	14.75	10.10	7.32	2.76
WSNR	(in)	21.86	20.27	19.66	19.34	19.13	18.60	17.37	16.81	16.49	16.28
	(sa)	79.26	72.00	66.39	63.31	66.57	51.18	41.91	36.55	32.91	30.28
	(na)	77.96	70.83	65.39	62.50	65.11	50.27	41.22	35.75	32.04	29.36
WSNRG	(in)	12.43	7.38	5.88	5.14	4.70	7.52	4.50	3.19	2.46	2.00
	(sa)	69.07	62.86	60.42	59.02	58.17	46.87	37.81	32.36	28.27	26.07
	(na)	67.68	61.21	58.46	57.26	55.41	45.51	36.67	30.97	26.84	24.39

TABLE 1. Quality measure values for the top left image in Figure 1.

		Motion Blur					Out-of-Focus Blur				
		R=2	R=3	R=4	R=5	R=6	P=3	P=5	P=7	P=9	P=11
SNR	(in)	26.72	23.12	21.06	19.57	18.38	23.71	21.45	19.92	18.69	17.65
	(sa)	59.38	54.96	53.10	51.24	50.10	37.87	33.14	31.50	29.90	27.71
	(na)	58.68	54.25	52.34	50.56	49.39	37.45	32.83	31.15	29.55	27.45
SNRG	(in)	7.48	3.62	2.34	1.72	1.38	4.12	2.50	1.83	1.44	1.16
	(sa)	39.62	36.45	35.65	33.22	32.36	18.03	13.87	11.88	10.13	7.87
	(na)	38.87	35.64	34.75	32.29	31.32	17.54	13.49	11.46	9.72	7.60
WSNR	(in)	17.60	14.96	13.77	13.03	12.51	15.34	13.85	13.08	12.54	12.10
	(sa)	58.76	55.37	53.37	51.46	49.35	33.34	27.96	26.14	24.14	22.81
	(na)	57.95	54.40	52.43	50.48	48.27	32.73	27.49	25.60	23.60	22.24
WSNRG	(in)	8.01	3.93	2.49	1.82	1.46	4.36	2.60	1.86	1.44	1.15
	(sa)	50.08	47.66	46.20	43.72	42.04	24.25	19.44	17.41	15.26	13.64
	(na)	49.16	46.40	44.90	42.26	40.40	23.44	18.72	16.57	14.38	12.71

TABLE 2. Quality measure values for the top right image in Figure 1.

results confirm that the spatially adaptive approach improves the quality of the restored image.

Moreover, several quantities involving the weighted or non-weighted quality measures of Section 5.1, can be defined for comparing the values of the weighted measures with those corresponding to the normal (*i.e.* non-weighted or global) measures, and in this way to quantify the advantage of using a spatially adaptive model. For example, one can compute

$$\text{M}_{out} - \text{M}_{in}, \tag{7}$$